Published by Nigerian Society of Physical Sciences. Hosted by FLAYOO Publishing House LTD

Recent Advances in Natural Sciences

Journal Homepage: https://flayoophl.com/journals/index.php/rans

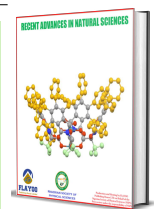

Baobab shell powder as a bio-filler in HDPE composites: mechanical, and physical properties

Daniel S. Sudi[a], Haruna P. Wante[b,*], Ndubuisi Mbada[a], Isah Baba[a], Bamidele Boluwatife[a], Solomon Adeleke[a]

[a]*Department of Metallurgical and Materials Engineering, Air Force Institute of Technology, Kaduna, Nigeria*
[b]*Plasma Technology Research Centre, Department of Physics, Faculty of Science, Universiti Malaya, Kuala Lumpur 50603, Malaysia*

ARTICLE INFO

Article history:
Received: 27 May 2025
Received in revised form: 19 July 2025
Accepted: 21 July 2025
Available online: 18 August 2025

Keywords: Baobab shell powder (BSP), Lignocellulosic materials, High-density polyethylene (HDPE), Bio-filler

DOI:10.61298/rans.2025.3.2.213

ABSTRACT

This study develops and characterizes high-density polyethylene (HDPE) composites reinforced with 0–20 wt% baobab shell powder (BSP) as a sustainable bio-filler. Composites were fabricated via compression molding and assessed for mechanical, physical, and chemical properties. XRF analysis revealed high metal oxide content in BSP—K_2O (29.32%), MgO (16.27%), CaO (12.42%), Al_2O_3 (12.12%), and SiO_2 (11.73%)—indicating multifunctional potential. FTIR confirmed lignocellulosic functional groups (O–H, C–H, C=O, C–O). Tensile strength peaked at 10.996 N/mm^2 (20 wt%, +6.14% vs. neat HDPE); yield strength peaked at 26.35 N/mm^2 (15 wt%), suggesting improved matrix interaction. Flexural strength dropped to 2.24 N/mm^2 at 10 wt% but stabilized thereafter; elongation at break fell from 37.74% to 7.87%, indicating increased rigidity. Impact energy dropped from 4.0 J to 1.63 J, while hardness and density rose from 11.36 to 28.66 N/m^2 and 0.87 to 0.93 g/cm^3, respectively. Water absorption remained low until day 6, then rose sharply to ~20% (20 wt%) by day 8 due to interfacial degradation. Composites with ≤10 wt% BSP showed better moisture resistance. The results demonstrated that BSP enhances stiffness, hardness, and tensile strength but reduces ductility and impact resistance, making it suitable for non-structural applications in automotive, packaging, and sustainable construction.

1. INTRODUCTION

In recent years, the pursuit of materials with enhanced and multifunctional properties has intensified, driven by the limitations of traditional ceramics, metals, and polymers [1]. As a result, researchers have increasingly turned their attention to composite materials. These engineered systems are formed by integrating two or more distinct components at the macroscopic level, each maintaining its inherent characteristics while contributing to the overall performance of the composite [2].

The demand for high-performance, cost-effective, and sustainable composite materials has significantly increased in recent years, driven by advancements in material science and the need for eco-friendly alternatives [3]. The renewable availability, high mechanical strength, low density, biodegradability, and diverse sources of cellulose make it a competitive material for polymer reinforcement [4]. High-Density Polyethylene (HDPE) is one of the most widely used thermoplastic polymers due to its superior

*Corresponding author Tel. No.: +234-806-4555-780
e-mail: wante2h@gmail.com (Haruna P. Wante)

mechanical strength, chemical resistance, and excellent processability [5]. However, like most polymers, HDPE exhibits limitations such as low stiffness, reduced thermal stability, and susceptibility to environmental degradation. To overcome these challenges, the incorporation of reinforcing fillers has been explored as an effective strategy to enhance the mechanical, thermal, and barrier properties of HDPE-based composites.

Conventionally, synthetic fillers such as glass fibers and carbon-based materials have been employed to reinforce polymer composites [6, 7]. However, these materials pose environmental concerns related to non-biodegradability, high energy consumption during production, and disposal challenges [8]. As a result, there has been a growing interest in utilizing natural fibers and bio-based fillers as sustainable alternatives. Among these, agricultural waste-derived fillers have gained considerable attention due to their availability, cost-effectiveness, and renewable nature.

Baobab shell powder (BSP), derived from the hard outer shell of the *Adansonia digitata* fruit, is an emerging bio-filler with promising attributes for composite reinforcement. It is abundant in the northern regions of Nigeria. Its fibers are derived from either the tree's pod or bark, carefully stripped from the lower trunk and husks. Additionally, the root bark serves as a valuable source of strong, durable fibers [9]. Rich in lignin, cellulose, and hemicellulose, baobab shell possesses high structural integrity, lightweight characteristics, and biodegradability, making it a suitable candidate for polymer reinforcement [10]. By incorporating BSP into HDPE, the resulting composite exhibit improved mechanical performance, physical stability, and environmental sustainability. Additionally, utilizing baobab shell, which is often discarded as agricultural waste, aligns with the principles of circular economy and waste valorization, reducing environmental impact and promoting resource efficiency.

This study aims to fabricate a HDPE composite reinforced with BSP, with a focus on its mechanical and physical properties. Various filler loadings were evaluated to identify the optimal composition that achieves a balance between strength, durability, and processability. The research contributes to the expanding field of natural fiber-reinforced polymer composites, offering a sustainable alternative for applications in packaging, construction, automotive components, and other engineering applications. The findings support the development of high-performance, eco-friendly materials that align environmental responsibility with industrial demands.

Although natural fillers such as rice husk [11, 12] and coconut shell [13, 14] have been extensively studied in polymer composites, the use of BSP in HDPE remains largely unexplored. As a lignocellulosic byproduct rich in reinforcing oxides like SiO_2, CaO, and MgO, baobab shell offers promising potential as a bio-filler in thermoplastics. We report for the first time, the investigation of HDPE composites reinforced with BSP, providing a detailed assessment of their mechanical and physical behavior across a filler loading range of 0–20 wt%. This work establishes crucial structure–property relationships and identifies the optimal filler content for achieving balanced performance in sustainable composite development.

2. MATERIALS AND METHODS

2.1. MATERIALS

The materials that were employed are ripe and matured baobab pods, HDPE, NaOH, pellets, digital weighing balance (Model No. D72336), ABG borosilicate glass beakers, filter paper and stirrers. Others are grinding machine, roll mill machine (Model No 5183), hydraulic press (Carver Incorporation New Jersey, U.S.A Model No 12000), tensile machine (Instron, model 3369, (CERD) No. 3369K1781), flexural testing machine (Serial No. Cat. Nr 261), impact testing machine (Capacity 15J and 25J, serial No. 412-07-15269C), and hardness testing machine (Vickers hardness tester, model: MV1-PC).

2.2. METHOD

2.2.1. Preparation, treatment and production of baobab shell powder and composite

Five (5) composite formulations containing BSP at varying filler loadings—0 wt%, 5 wt%, 10 wt%, 15 wt%, and 20 wt%—were fabricated using a standardized molding process. For each composition, three (3) test specimens were prepared following the relevant dimensional standards for physical and mechanical property evaluations. The average values were plotted, and the standard deviations were calculated and represented as error bars. All samples were systematically coded to facilitate accurate identification and traceability during testing.

The filler material was obtained from baobab shells collected from mature and fully ripened baobab pods. These pods were sourced from baobab trees located in Katsina, Katsina State, Nigeria (Figure 1). The pods were mechanically sliced open, and the shells were manually separated from the fruit pulp. The separated shells were thoroughly washed first with tap water, then with distilled water, and subsequently air-dried at ambient conditions. To improve the surface and bonding properties of the shell material, an alkaline pretreatment was applied, following the general approach summarized by Li *et al.* [15]. The air-dried baobab shells were subjected to an alkali pretreatment by immersing them in a 6 wt% sodium hydroxide (NaOH) solution at ambient temperature (approximately 25 °C) for 1 hour under gentle stirring to ensure uniform exposure. This alkaline treatment is known to disrupt the ester bonds between lignin, hemicellulose, and cellulose, effectively removing amorphous components such as lignin, hemicellulose, pectin, and surface waxes. The process enhances the porosity and surface reactivity of the biomass, improving its physicochemical properties for subsequent applications. After treatment, the shells were thoroughly rinsed multiple times with distilled water until a neutral pH (pH ~7) was attained, indicating the complete removal of residual alkali. Finally, the pretreated shells were air-dried at room temperature for 24 hours to eliminate moisture and residual chemicals, yielding a cleaner and more reactive surface structure.

Following the drying step, the shells were ground using a locally fabricated milling machine to reduce their size. The resulting powder was sieved through a 1 mm mesh to achieve a uniform particle size distribution suitable for composite fabrication. A schematic representation of the baobab shell processing steps is provided in Figure 2.

The HDPE and sieved BSP were used to fabricate the composites. The compounding process was carried out using a two-roll mill (preheated to 135 °C for 30 minutes), corresponding to the

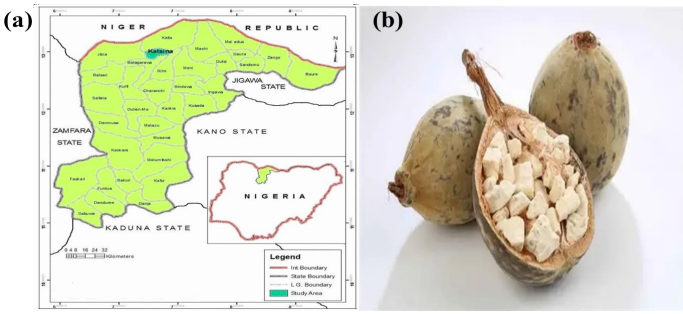

Figure 1. Map of Nigeria indicating Katsina State, the source location of the baobab pods (adapted from Badr [16]); (b) Image of harvested baobab pods.

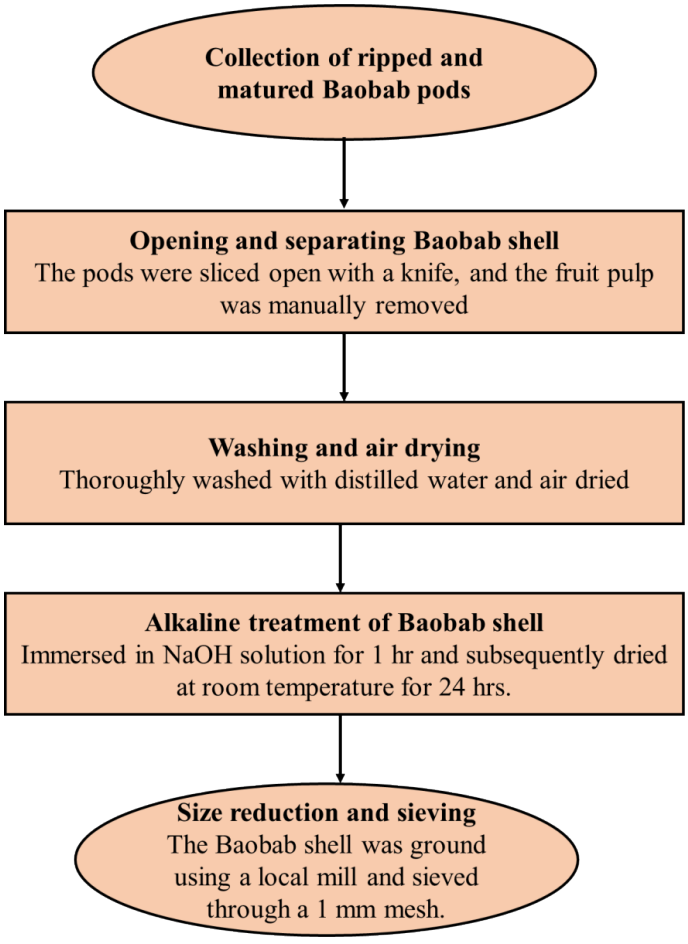

Figure 2. Schematic diagram of the processing steps for baobab shell preparation, including collection, mechanical opening, washing, alkaline treatment, and size reduction.

melting temperature of HDPE. Initially, 95 wt% of HDPE was introduced and allowed to melt uniformly for approximately 5 minutes. Subsequently, 5 wt% of BSP was gradually incorporated into the molten polymer, ensuring homogeneous dispersion throughout the matrix. The compounded material was then retrieved from the mill in the form of a continuous sheet. Compression molding was employed to form the final composite specimens. The BSP/HDPE sheet was placed into a rectangular mold with internal dimensions of 100 mm × 120 mm × 3 mm, lined with aluminum foil to prevent adhesion. The molding assembly was transferred into a preheated compression molding press maintained at 135 °C. A uniaxial load of 10 kN was applied for 6 minutes to facilitate proper consolidation. Upon completion, the mold was removed and cooled to ambient conditions before demolding the solidified composite.

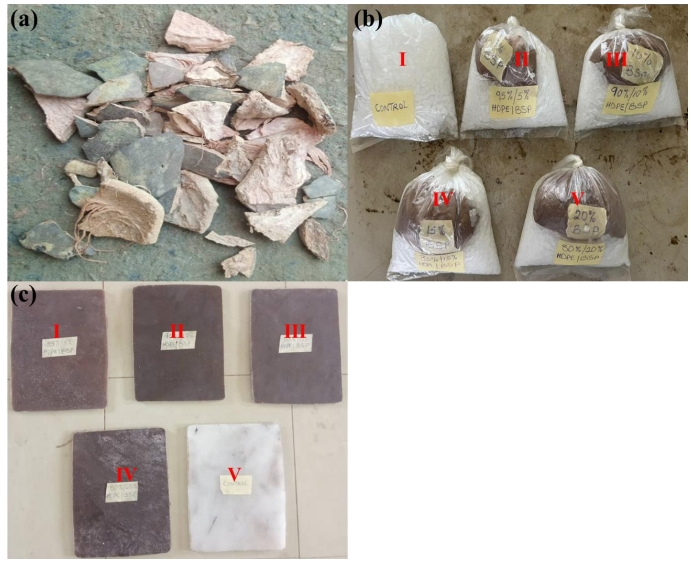

Figure 3. (a) Reduced size baobab shells; (b) Prepared composition of BSP/HDPE for (i) 0:100wt%, (ii) 5:95wt%, (iii) 10:90wt%, (iv)15:85wt%, and (v) 20:80wt%; (c) Produced rectangular composite sheet of BSP/HDPE matrixes for (i) 5:95wt%, (ii) 10:90wt%, (iii)15:85wt%, (iv) 20:80wt% and (v) 0:100wt%.

This protocol was replicated for additional formulations with BSP loadings of 10, 15, and 20 wt%, corresponding to HDPE matrix contents of 90, 85, and 80 wt%, respectively. A neat HDPE sample (100 wt%) served as the control. Images of the resulting composite sheets are presented in Figure 3.

2.2.2. Mechanical tests

The mechanical properties of the developed samples, including tensile strength, flexural strength, impact energy, hardness, and percentage elongation, were evaluated. Tensile testing was performed according to ASTM D638 using an Instron universal testing machine. Standard test specimens were gripped at both ends and subjected to a continuously increasing uniaxial load until fracture. The tensile strength was determined by dividing the maximum load by the cross-sectional area, while the modulus of elasticity was calculated as the stress-to-strain ratio. Percentage elongation at break was measured as the percentage change in specimen length at fracture.

Flexural strength, representing a material's resistance to bending, was assessed via a three-point bending test following ASTM D790. Rectangular specimens (100 mm × 20 mm × 10 mm) were tested with a span length of 100 mm and a strain rate of 5 mm/min. Flexural strength was computed using eq. (1) [17]:

$$MOR = \frac{3PS}{2bt^2}, \tag{1}$$

where S is the length of support span (measured in mm), P is the load applied (kN), b is the width of the specimen (measured in mm), and t is the thickness of specimen (measured in mm).

The impact test was conducted according to ASTM D256 using a Charpy V-notch impact testing machine. The dimensions, gauge length, and V-notch were selected based on the standard. Each specimen was positioned in a specialized holder with the notch oriented vertically and facing the impact point. The specimen was then struck by a tip attached to a swinging pendulum. Upon impact, the specimen fractured at its notched cross-section, and the upward swing of the pendulum was used to determine the energy absorbed during the process.

The hardness test was performed according to ASTM D2240 using a Shore durometer testing machine. The sample dimensions and gauge length were selected in accordance with the standard. Each sample was cut into 25 × 25 × 10 mm square strips for testing. The test involved gradually pressing a presser foot with a diamond-tipped indenter into the specimen. The hardness value was determined based on the depth of penetration of the indenter into the sample.

2.2.3. Physical tests

Density determination

The densities of the samples were determined by measuring their weight using a digital weighing balance and calculating their volume. Density was then computed using the following eq. (2):

$$\rho = \frac{m}{V}, \tag{2}$$

where m is the mass, V is the volume, and ρ is the density (g/cm^3).

Water absorption test

This test measures a material's moisture absorption in a humid environment. Samples were first dried in an oven at 60°C for 4 hours, then placed in a desiccator for another 4 hours to stabilize their weight. After weighing, they were submerged in a 250 ml beaker of water for 24 hours. Following immersion, the samples were removed, dried, and reweighed according to ASTM D570-98. The percentage of water absorbed was then calculated using eq. (3) [18]:

$$\%\ \text{of water absorbed} = \frac{w_f - w_i}{w_i} \times 100, \tag{3}$$

where w_f is the weight of the sample after immersion in water and w_i is the weight of the sample before immersion in water.

3. CHARACTERIZATION

The elemental composition of BSP was analyzed using an Energy Dispersive X-ray Fluorescence (EDXRF (EDX3500 benchtop)) spectrometer. The powder was pressed into a pellet and examined under vacuum conditions, with XRF data recorded over 0–40 keV. Functional groups were identified using a benchtop Fourier Transform Infrared (FTIR, 630) spectrometer with a diamond ATR accessory. The powder was placed on the ATR crystal and analyzed over a wavenumber range of 4000–400 cm^{-1}.

4. RESULTS AND DISCUSSION

4.1. XRF ANALYSIS

Figure 4 presents the XRF composition of the BSP revealing a composition rich in various metal oxides, indicating its potential for multiple applications, including refractory materials, polymer reinforcement, catalysis, and adsorption processes [19]. The dominant oxides present are potassium oxide (K_2O, 29.32%), magnesium oxide (MgO, 16.27%), calcium oxide (CaO, 11.50%), aluminium oxide (Al_2O_3, 12.12%), and silicon dioxide (SiO_2, 11.73%), all of which contribute to the material's thermal stability, mechanical strength, and chemical reactivity [20]. The high SiO_2 and Al_2O_3 content suggests that baobab shell-derived materials could be used in ceramic composites, refractory linings, and heat-resistant coatings, enhancing their durability under high-temperature conditions [21, 22]. Additionally, these oxides, along with CaO and MgO, can reinforce polymer matrices [23], improving mechanical properties, fire resistance, and stability in composite materials.

Beyond structural applications, the presence of transition metal oxides, including iron oxide (Fe_2O_3, 4.68%), manganese oxide (MnO, 0.25%), copper oxide (CuO, 1.29%), cobalt oxide (CoO, 0.15%), and chromium oxide (Cr_2O_3, 0.27%), suggests potential catalytic activity in redox reactions [24], pollutant degradation, and hydrogen production [25]. These oxides, particularly Fe_2O_3 and CuO, are known for their adsorptive and catalytic properties [26], making the material suitable for wastewater treatment, gas adsorption, and chemical processing. The presence of phosphorus pentoxide (P_2O_5, 1.48%) and sulfur trioxide (SO_3, 3.08%) further supports its adsorption potential [27].

For electrical and energy storage applications, oxides such as tantalum pentoxide (Ta_2O_5, 0.03%), tungsten oxide (WO_3, 0.05%), niobium oxide (Nb_2O_5, 0.12%), and cobalt oxide (CoO, 0.15%) indicate that the material could have applications in electronic devices, capacitors, and energy storage systems [28, 29]. The high potassium content (K_2O, 29.32%) may also influence ionic conductivity, making it relevant for electrochemical applications. The trace amounts of zirconium oxide (ZrO_2, 0.13%) and tin oxide (SnO_2, 0.17%) contribute to high-temperature resistance and wear resistance, which are essential for ceramics, coatings, and advanced composites [30].

The rich oxide profile of BSP positions it as an effective multifunctional filler for advanced composites. Key oxides like SiO_2, Al_2O_3, CaO, and MgO enhance thermal stability, mechanical strength, and interfacial bonding in polymer matrices [31]. Meanwhile, trace transition metal oxides (Fe_2O_3, CuO, CoO, Ta_2O_5) provide catalytic and electrochemical properties, enabling hybrid composites with combined structural and functional capabilities [32]. This makes BSP a sustainable, cost-effective bio-based additive for high-performance materials in energy storage, catalysis, and structural applications.

4.2. FUNCTIONALIZATION ANALYSIS

Figure 5 displays the FTIR spectrum of BSP, elucidating the complex chemical functionalities inherent in its lignocellulosic structure. The broad, intense band centered around 3280 cm^{-1} corresponds to O–H stretching vibrations, which are typically associated with hydrogen-bonded hydroxyl groups prevalent in cellulose, hemicellulose, and lignin [33]. This broadness is indicative of extensive intra- and intermolecular hydrogen bonding, a hallmark of highly polar biopolymers [34].

The absorption band at ~2918 cm^{-1} is attributed to asymmetric and symmetric C–H stretching vibrations of –CH_2 and –CH_3 groups, confirming the presence of aliphatic hydrocarbons, particularly in the side chains of cellulose and hemicellulose [35].

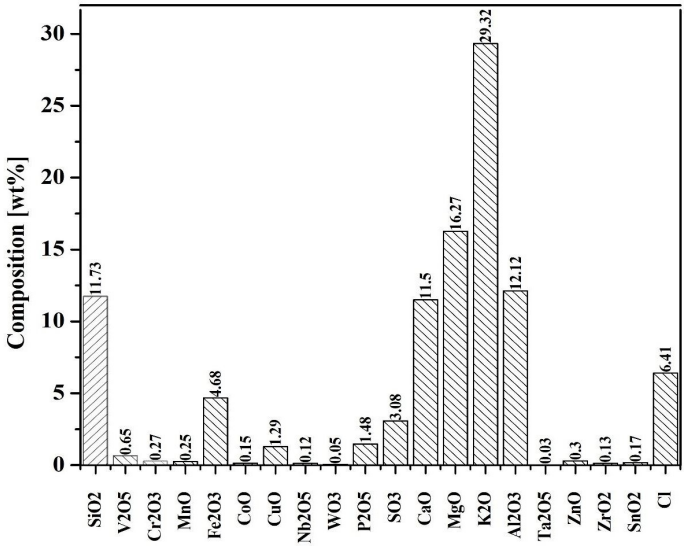

Figure 4. Elemental oxide profile of BSP determined by XRF analysis, showing composition in weight percent (wt%).

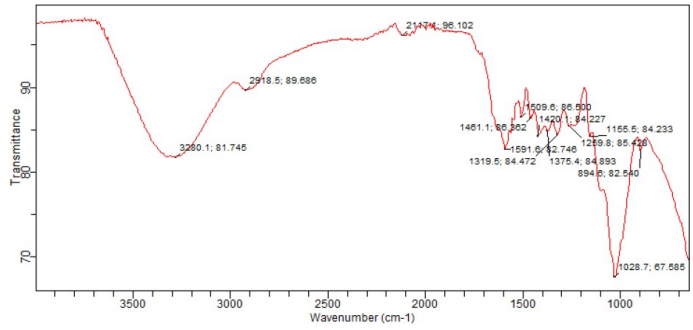

Figure 5. Functionalization spectrum of BSP.

The small but distinct peak near 2147 cm^{-1} may correspond to C≡C (alkyne) or C≡N (nitrile) stretching modes, suggesting minor contributions from unsaturated or nitrogen-containing groups, possibly originating from protein residues or environmental exposure [36].

Peaks at 1591 cm^{-1} and 1461 cm^{-1} are associated with aromatic C=C stretching, indicative of the phenylpropanoid unit's characteristic of lignin. These vibrations confirm the aromatic backbone structure typical of lignin's guaiacyl and syringyl units. The band at ~1481 cm^{-1} could also represent symmetric bending vibrations of $–CH_3$ groups attached to the aromatic rings [37]. The 1375 cm^{-1} band is ascribed to C–H deformation (bending) in cellulose and hemicellulose, while the 1259 cm^{-1} absorption peak signifies C–O stretching in aryl ethers and esters, again pointing to lignin and hemicellulosic ester linkages.

A prominent absorption band at ~1028 cm^{-1} corresponds to C–O–C stretching vibrations in pyranose rings, a strong indicator of the glycosidic bonds in cellulose and hemicellulose. Meanwhile, the peak at 894 cm^{-1} represents β-glycosidic linkages (β-1,4), a defining structural motif of cellulose, further validating the polysaccharide-rich nature of the biomass [38].

Collectively, these spectral signatures confirm that the BSP comprises a robust lignocellulosic matrix, with distinct contributions from cellulose, hemicellulose, and lignin. This chemical fingerprint not only confirms its suitability for valorization in bio-based composites, adsorbents, or functionalized materials but also aligns with literature reports on other plant-derived biomass [33].

4.3. MECHANICAL PROPERTIES

4.3.1. Tensile strength and percentage of elongation

Figure 6a presents the variation in tensile strength of HDPE composites as a function of BSP loading. The neat HDPE matrix (0 wt% BSP) exhibits a tensile strength of 10.36 N/mm^2, which is consistent with values reported in prior literature for commercially processed HDPE [39]. This baseline reflects HDPE's inherent strength, attributed to its semicrystalline structure and effective polymer chain entanglement, which resist tensile deformation.

The introduction of 5 wt% BSP results in a moderate decrease in tensile strength to 10.052 N/mm^2, corresponding to a 2.97% reduction relative to neat HDPE. A further decline to 9.758 N/mm^2 is observed at 10 wt% BSP loading, indicating an overall 5.81% decrease from the neat polymer.

These initial reductions in tensile performance can be primarily ascribed to the inadequate interfacial adhesion between the hydrophilic BSP particles—rich in cellulose, hemicellulose, and lignin—and the hydrophobic HDPE matrix [40]. This incompatibility weakens filler-matrix bonding, hindering load transfer and promoting particle agglomeration, which creates stress points that trigger microcracks under tension [41]. Similar observations were noted by Uzochukwu & Eze [40] in their study of physico-mechanical properties of treated baobab fiber (*Adansonia Digitata*) nano-filler/epoxy composite and Shakuntala & Raghavendra [42] beyond a certain threshold.

At 15 wt% BSP, tensile strength recovers to 10.082 N/mm^2—just 2.68% below neat HDPE— suggesting improved filler dispersion and interfacial bonding. This results in a more uniform microstructure and better stress distribution. The recovery likely indicates a percolation threshold, where filler networking enhances the composite's mechanical integrity.

The highest tensile strength is achieved at 20 wt% BSP, reaching 10.996 N/mm^2—a 6.14% increase over neat HDPE. This improvement is likely attributed to synergistic effects: (i) effective dispersion and mechanical interlocking of filler particles enhance stress transfer from the HDPE matrix to the rigid filler phase; (ii) the intrinsic stiffness of lignocellulosic particles reinforces the matrix by restricting polymer chain mobility; and (iii) the microstructural features of the filler likely act as nucleating sites, promoting localized crystallinity and contributing to the overall stiffness and strength of the composite [43, 44].

This reflects a typical non-monotonic behaviour in particulate-reinforced thermoplastic composites [45, 46]. At low filler loadings, poor compatibility and filler agglomeration dominate, reducing mechanical performance. However, as the filler content approaches an optimum threshold, improved particle distribution and interfacial bonding begin to outweigh these detrimental effects, leading to mechanical enhancement. The peak performance at 20 wt% BSP suggests that this is the optimal filler loading under the current processing conditions to achieve max-

imum reinforcement without compromising the integrity of the polymer network.

Figure 6b shows the variation in percentage elongation of HDPE composites with increasing BSP content. Elongation at break is a key indicator of ductility, reflecting the material's ability to deform plastically before failure—crucial for applications requiring flexibility and impact resistance [47].

Neat HDPE (0 wt% BSP) exhibits a high elongation at break of 37.74%, reflecting its inherently ductile thermoplastic nature due to the slippage and realignment of semi-crystalline molecular chains under tensile stress. With the addition of 5 wt% BSP, elongation drops sharply to 15.99%— a 57.6% reduction. This decline in ductility is likely attributed to the rigid lignocellulosic filler, which hinders polymer chain mobility. Moreover, poor interfacial bonding and potential filler agglomeration at low loadings may introduce stress concentrations, leading to early crack initiation and reduced deformation capacity.

At 10 wt% BSP, elongation further decreases to 8.24%, reflecting increased composite rigidity. The added filler restricts HDPE chain mobility, resulting in a stiffer matrix with reduced strain tolerance—consistent with trends observed in other natural fiber-reinforced polymers [41, 43]. Interestingly, at 15 wt%, elongation rises slightly to 10.54%. This anomaly may be due to improved filler dispersion and stronger filler–matrix interactions at this concentration, which minimize stress concentrations and promote better energy absorption during deformation. The enhanced interfacial bonding at 15 wt% likely contributes to the observed increase in ductility and toughness.

At 20 wt% BSP, elongation declines to 7.87%, reinforcing the trend that higher filler content reduces ductility [48]. Despite this reduction, the tensile strength reaches a peak of 10.996 N/mm^2 (Figure 6a), indicating an inverse relationship between tensile strength and elongation. The increase in tensile strength is attributed to enhanced filler–matrix adhesion and effective stress transfer. However, these same factors restrict polymer chain mobility and increase the composite's rigidity, thereby limiting its ability to undergo plastic deformation.

This mechanical behaviour reflects the classic stiffness-ductility trade-off in polymer composites: rigid fillers enhance strength and stiffness but constrain ductility when well dispersed and well bonded. The results at 20 wt% BSP illustrate this balance, emphasizing the need to tailor filler content based on application requirements. While 15–20 wt% BSP enhances tensile performance, it compromises elongation, highlighting the necessity of optimizing filler levels to achieve a suitable balance between strength, stiffness, and flexibility for specific end-use applications.

4.3.2. Yield and flexural strengths

Figure 7a illustrates the yield strength variation of HDPE composites as a function of BSP content, ranging from 0 to 20 wt%. The neat HDPE matrix (0:100) demonstrates the highest yield strength at 94.35 N/mm^2, providing the baseline mechanical performance of the unreinforced polymer. Upon the addition of 5 wt% BSP, the yield strength experiences a sharp decline to 39.99 N/mm^2, corresponding to a 57.6% drop from the neat HDPE. This significant decline is likely attributed to two primary factors: the reduction in polymer chain mobility due to filler incorporation and the inadequate interfacial bonding between the hydrophobic HDPE matrix and the hydrophilic BSP particles [49]. These mechanisms hinder effective stress transfer under load, resulting in premature yielding.

Increasing BSP content to 10 wt% causes yield strength to drop sharply to 20.60 N/mm^2—a 78.2% reduction from neat HDPE—likely due to filler agglomeration, voids, and stress concentrations that disrupt matrix continuity and load transfer. At 15 wt%, yield strength recovers to 26.35 N/mm^2 (27.9% increase from 10 wt%), likely from improved filler dispersion and interfacial bonding near a percolation threshold enhancing matrix–filler synergy. However, at 20 wt%, yield strength decreases again to 19.68 N/mm^2 (25.3% decline from 15 wt%), indicating excessive filler leads to agglomeration and defects that compromise mechanical integrity.

The yield strength results show a non-linear, generally decreasing trend with increasing BSP content, highlighting that low filler loadings can reinforce polymers, but excessive unmodified filler weakens composite integrity. Similar observation was noted by Kaurase & Singh [50] in their study on poly (vinyl alcohol) (PVA) composites reinforced with cellulosic fibres derived from *Delonix regia* fruits. This underscores the complex relationship between filler content and mechanical performance in natural fibre-reinforced composites. The findings emphasize the importance of surface treatments or compatibilizers to improve interfacial adhesion and stress transfer at the filler–matrix interface, which is essential for achieving high-performance composite materials.

Figure 7b shows that the neat HDPE has the highest flexural strength of 2.86 N/mm^2, which slightly decreases to 2.71 N/mm^2 at 5 wt% BSP. This minor reduction likely indicates that low filler content does not significantly impair the matrix's bending resistance or induce brittleness. At 10 wt% BSP, flexural strength drops to 2.24 N/mm^2, likely due to interfacial debonding and microstructural heterogeneity that restrict polymer chain mobility and create crack-prone areas. However, flexural strength slightly recovers at 15 wt% (2.34 N/mm^2) and 20 wt% (2.37 N/mm^2), suggesting improved filler interlocking and stress redistribution.

Unlike the sharp decline in yield strength, flexural strength shows a moderate decrease followed by stabilization, indicating greater tolerance to structural heterogeneity under bending loads. This aligns with hardness trends (Figure 8b), where increased filler content steadily stiffens the matrix, enhancing flexural performance under static stress.

The yield and flexural strength profiles reveal how BSP content differently affects the composite's mechanical behaviour. Yield strength is highly sensitive to filler dispersion and matrix integrity, while flexural strength benefits from increased stiffness at higher loadings. This contrasts with impact strength, which steadily declines, reflecting increased brittleness, and parallels the continuous hardness improvement with BSP addition.

Notably, 15 wt% BSP appears to represent a transitional point, where both yield and flexural strengths begin to recover—indicating improved filler dispersion or partial interfacial compatibility. However, at 20 wt% BSP, while flexural strength continues to increase slightly, yield strength declines again, suggesting that excessive filler content may compromise matrix continuity or stress transfer efficiency.

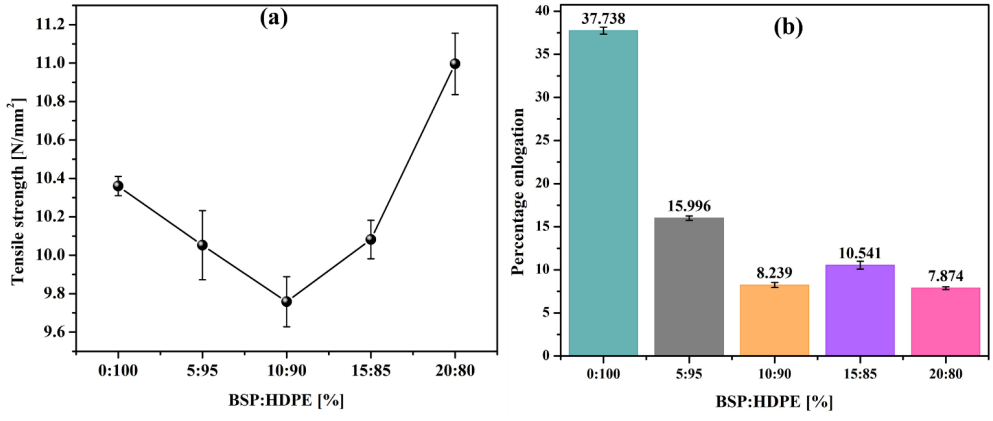

Figure 6. Variation of (a) tensile strength with filler loading composition in BSP reinforced HDPE composite; (b) percentage elongation with filler loading composition in BSP reinforced HDPE composite.

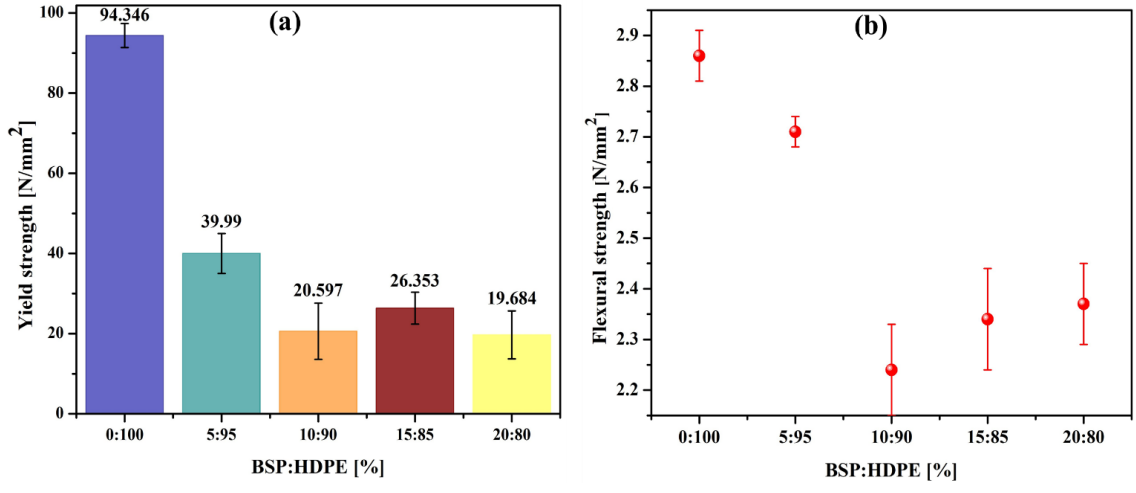

Figure 7. Variation of (a) yield strength and (b) flexural strength with filler loading composition in BSP reinforced HDPE composite.

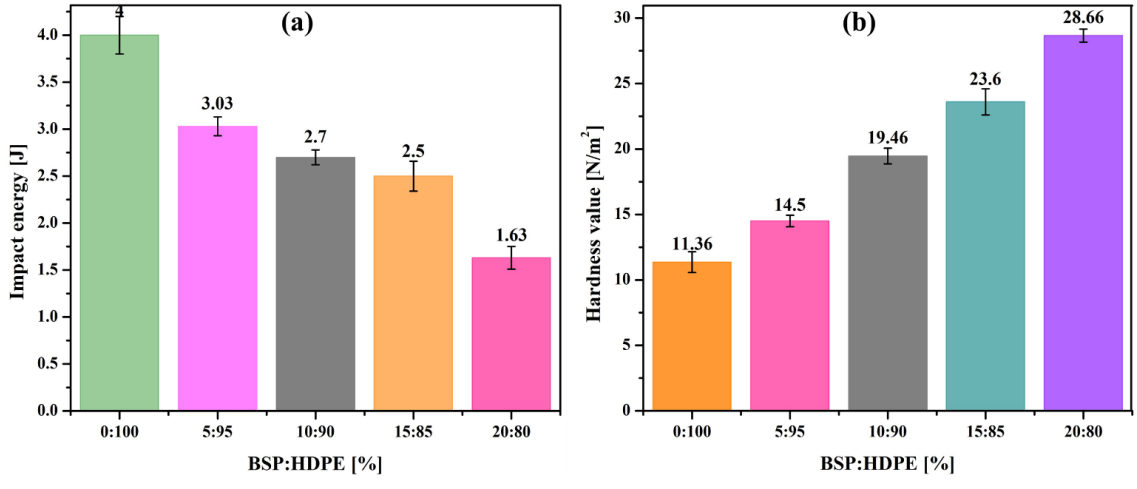

Figure 8. Variation of (a) impact energy and (b) hardness values with filler loading composition in BSP reinforced HDPE composite.

4.3.3. Impact energy and hardness

The impact energy profile of HDPE composites reinforced with varying contents of BSP reveals a consistent decline in impact resistance as filler loading increases, as depicted in Figure 8a. The neat HDPE sample (0 wt% BSP) exhibits the highest impact energy value of 4.0 J, indicative of its superior toughness and ductile nature, which allows efficient energy absorption under sudden loading. However, as the proportion of BSP increases, a gradual reduction in impact energy is observed, with values decreasing to 3.03 J, 2.7 J, 2.5 J, and 1.63 J for 5 wt%, 10 wt%,

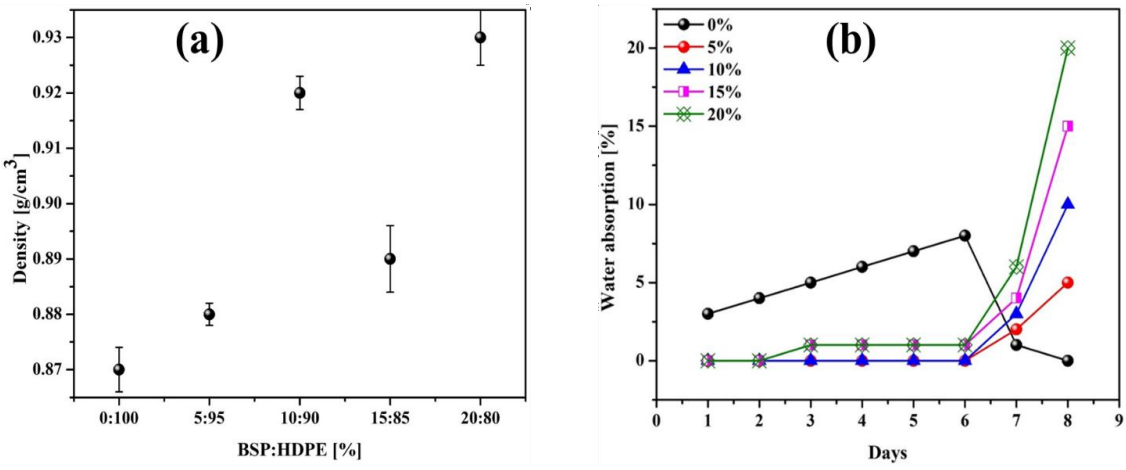

Figure 9. Variation of (a) density with filler loading composition in BSP reinforced HDPE composite; (b) water absorption with time (days) on filler loading of BSP reinforced HDPE composite.

15 wt%, and 20 wt% filler loadings, respectively.

This result is consistent with the commonly reported phenomenon where natural filler reinforcement in polymer matrices leads to a deterioration in impact strength [51, 52]. The progressive reduction in impact energy is likely attributed to the restricted molecular mobility of the HDPE chains caused by the presence of rigid filler particles. As the BSP content increases, the matrix becomes stiffer, which limits its ability to undergo plastic deformation and absorb impact forces effectively. This mechanical stiffening is advantageous for load-bearing applications but negatively affects the material's energy dissipation capability under dynamic stress conditions.

The interfacial adhesion between BSP and the HDPE matrix is likely suboptimal due to polarity differences—BSP being hydrophilic and HDPE hydrophobic. This mismatch can lead to poor bonding, void formation, and micro-gaps at the interface, which act as stress concentrators under impact loading, promoting early crack initiation and propagation.

At higher BSP loadings, particle agglomeration further contributes to localized stress zones and microcrack formation [53], degrading impact performance. Particle morphology also plays a role—irregular or angular particles induce sharper stress fields, lowering toughness compared to well-dispersed, rounded particles [54]. Moreover, the intrinsic brittleness of BSP limits its ability to absorb impact energy [52], unlike elastomeric fillers. While it reinforces stiffness and hardness, its lack of deformability reduces impact resistance.

Nevertheless, BSP enhances properties like rigidity, dimensional stability, and hardness, making it suitable for static applications. Hence, optimizing the balance between stiffness and toughness is essential, depending on the intended application.

The hardness of HDPE composites increases consistently with rising BSP content, as shown in Figure 8b. Neat HDPE exhibits the lowest hardness (11.36), while composites with 5 wt%, 10 wt%, 15 wt%, and 20 wt% BSP show progressive increases to 14.5, 19.46, 23.6, and 28.66, respectively. This trend reflects the stiffening effect of BSP, which restricts HDPE chain mobility and enhances resistance to localized deformation. The improvement is attributed to the inherent rigidity and structural integrity of BSP, which reinforces the matrix and reduces plastic flow under indentation. Fine, well-dispersed BSP particles also promote mechanical interlocking and act as localized barriers to surface penetration, enhancing wear resistance [55]. This enhancement is likely due to the stiffening effect of the BSP and the increased cross-link density formed between the baobab particles and the epoxy chains [40]. Similar observation was reported by Uzochukwu & Eze [40].

Despite the potential for agglomeration at higher loadings, the continued rise in hardness suggests effective dispersion and minimal adverse filler–filler interactions. This makes HDPE–BSP composites suitable for applications requiring enhanced surface durability, such as automotive interiors, flooring, and industrial components.

While hardness improves with increasing BSP content, this enhancement does not extend uniformly across all mechanical properties. Impact energy decreases significantly (Figure 8a), and tensile strength (Figure 6a) initially drops before peaking at 20 wt% filler. These contrasting trends underscore that, rigid fillers enhance surface resistance (e.g., hardness) but often compromise ductility and energy absorption. Moreover, the rise in hardness may lead to increased brittleness, raising concerns under dynamic or flexural loads. At higher filler loadings, particle agglomeration and poor interfacial adhesion can create stress concentrators, promoting crack initiation.

4.4. PHYSICAL PROPERTIES

4.4.1. Density and water absorption

The density of HDPE composites reinforced with BSP increases with filler content (Figure 9a), reflecting the higher specific gravity of BSP compared to HDPE. Neat HDPE (0 wt%) shows the lowest density (0.87 g/cm^3), while 5, 10, 15, and 20 wt% BSP composites exhibit densities of 0.88, 0.92, 0.89, and 0.93 g/cm^3, respectively. The slight dip at 15 wt% likely results from filler agglomeration or voids disrupting uniform packing.

This density trend correlates with mechanical performance. Tensile strength initially decreases due to weak interfacial bonding but recovers at 20 wt%, aligning with maximum density. Impact energy declines steadily (from 4.0 J to 1.63 J), indicating

increased brittleness due to reduced chain mobility and higher filler content. Hardness increases from 11.36 to 28.66, closely following the density rise and reflecting enhanced stiffness and surface resistance.

Increasing BSP content shifts the composite toward a denser, stiffer material with improved hardness and tensile strength at higher loadings, but reduced impact resistance. This trade-off informs application suitability: higher density favors structural uses (e.g., automotive, construction), while lower density is better for impact-sensitive applications. Enhancing filler dispersion or applying compatibilizers may further optimize performance by improving interfacial bonding.

The variation in water absorption over time for BSP-reinforced HDPE composites highlights the influence of filler loading on the material's water resistance (Figure 9b). Figure 9b illustrates how different filler concentrations (0%, 5%, 10%, 15%, and 20%) affect the percentage of water absorbed over an 8-day period. The behaviour observed indicates that while HDPE is inherently hydrophobic, the introduction of BSP significantly alters its water absorption characteristics, especially at higher filler loadings.

For the neat HDPE (0% BSP) sample, a steady increase in water absorption is observed over the first 6 days, peaking at ca. 7.5%. This gradual absorption aligns with HDPE's low intrinsic affinity for water, confirming its hydrophobic nature [56]. Similar trend was also observed by Uzochukwu & Eze [40]. However, a sharp decline on day 7 suggests possible material saturation, surface water evaporation, or the diffusion of water out of the composite structure. Since HDPE has a non-polar molecular structure [57], it does not readily interact with water, and any minor absorption may be due to surface irregularities rather than bulk penetration.

For 5% and 10% filler composites, water absorption remains low for the first 6 days, similar to pure HDPE. After day 6, absorption rises sharply—especially in the 10% sample, reaching ~10% by day 8. This indicates that initial polymer resistance to moisture is compromised over time due to weak polymer-filler interfacial bonding, leading to microcrack formation and water diffusion [58].

At 15% and 20% filler loadings, water absorption is negligible initially but increases rapidly after day 6, with the 20% composite absorbing nearly 20% by day 8. This surge reflects increased moisture pathways from the porous BSP and greater filler-polymer interfacial area. The hydrophilic nature of the filler further accelerates water uptake at higher loadings, undermining long-term moisture resistance.

The threshold effect observed at day 6 is significant. Initially, composites show minimal water absorption, but beyond a critical exposure point, absorption rises sharply—likely due to polymer-filler interfacial degradation, filler swelling, or void formation that facilitates water ingress. Higher filler content reduces the matrix's ability to encapsulate particles, increasing diffusion pathways. Structurally, composites with ≤10% filler maintain water resistance longer, suitable for moderate moisture conditions. In contrast, ≥15% filler leads to rapid water uptake, threatening long-term durability through swelling, dimensional instability, and strength loss.

Enhancing water resistance at high filler loadings requires surface treatments, chemical modifications, or hydrophobic compatibilizers—such as silane coupling agents, plasma treatments, or polymer grafting—to improve interfacial bonding and reduce permeability. Optimizing processing and filler dispersion can also minimize voids and moisture ingress.

While BSP improves certain properties, high loadings compromise water resistance, suggesting lower filler content or additional treatments for applications demanding long-term moisture stability.

5. CONCLUSION

This study demonstrated that BSP is an effective and sustainable bio-filler for enhancing the mechanical and physical properties of HDPE composites. BSP increased tensile strength (up to 10.996 N/mm^2 at 20 wt%), hardness (from 11.36 to 28.66), and density (from 0.87 to 0.93 g/cm^3), indicating improved rigidity and surface resistance. However, these gains came at the expense of ductility and impact strength, which decreased significantly with filler loading—highlighting a clear stiffness–toughness trade-off.

Water absorption results showed a threshold behaviour, with significant uptake after prolonged exposure, especially at ≥15 wt% filler content, due to interfacial degradation and filler porosity. Despite this, composites with ≤10 wt% BSP maintained better moisture resistance, while the 15 wt% composite exhibited the best balance between strength, hardness, and flexibility.

BSP-reinforced HDPE composites are suitable for non-structural applications requiring moderate strength and rigidity, such as packaging, interior automotive components, and eco-friendly building materials. Further improvements in moisture resistance and interfacial bonding through surface modification or compatibilizers are recommended to expand their applicability in more demanding environments.

DATA AVAILABILITY STATEMENT

The data are available with the corresponding author upon request.

References

[1] R. G. Mandala, D. Hegde, V. R. Kodali & V. R. Kode, "From waste to strength: Unveiling the mechanical properties of peanut-shell-based polymer composites", Journal of Composites Science **7** (2023) 307. https://doi.org/10.3390/jcs7080307.

[2] H. T. N. Kuan, M. Y. Tan, Y. Shen & M. Y. Yahya, "Mechanical properties of particulate organic natural filler-reinforced polymer composite: A review", Composites and Advanced Materials **30** (2021) 26349833211007502. https://doi.org/10.1177/26349833211007502.

[3] T. K. Das, P. Ghosh & N. C. Das, "Preparation, development, outcomes, and application versatility of carbon fiber-based polymer composites: a review", Advanced Composites and Hybrid Materials **2** (2019) 214. https://doi.org/10.1007/s42114-018-0072-z.

[4] J. Oboh, J. Okafor, A. Kovo & A. Abdulrahman, "Investigation of eco-friendly cellulosic nanoparticles potential as reinforcement agent in the production of natural rubber composites", Nigerian Journal of Technology **36** (2017) 1078. DOI:10.4314/njt.v36i4.13.

[5] M. Y. Khalid, A. Al Rashid, Z. U. Arif, W. Ahmed, H. Arshad & A. A. Zaidi, "Natural fiber reinforced composites: Sustainable materials for emerging applications", Results in Engineering **11** (2021) 100263. https://doi.org/10.1016/j.rineng.2021.100263.

[6] S. Araby, B. Philips, Q. Meng, J. Ma, T. Laoui & C. H. Wang, "Recent advances in carbon-based nanomaterials for flame retardant polymers and composites", Composites Part B: Engineering **212** (2021) 108675. https://doi.org/10.1016/j.compositesb.2021.108675.

[7] M. Harussani, S. Sapuan, G. Nadeem, T. Rafin & W. Kirubaanand, "Recent applications of carbon-based composites in defence industry: A review",

Defence Technology **18** (2022) 1281. https://doi.org/10.1016/j.dt.2022.03.006.

[8] A. Soni, P. K. Das, S. K. Gupta, A. Saha, S. Rajendran, H. Kamyab & M. Yusuf, "An overview of recent trends and future prospects of sustainable natural fiber-reinforced polymeric composites for tribological applications", Industrial Crops and Products **222** (2024) 119501. https://doi.org/10.1016/j.indcrop.2024.119501.

[9] M. Sidibe & J. T. Williams, *Baobab, Adansonia Digitata L*, Crops for the Future Series, International Centre for Underutilised Crops, 2002. https://books.google.com.ng/books?id=zskefIIlc1IC.

[10] A. H. Birniwa, S. S. Abdullahi, M. Ali, R. E. A. Mohammad, A. H. Jagaba, M. Amran, S. Avudaiappan, N. Maureira-Carsalade & E. I. S. Flores, "Recent trends in treatment and fabrication of plant-based fiber-reinforced epoxy composite: a review", Journal of Composites Science **7** (2023) 120. https://doi.org/10.3390/jcs7030120.

[11] J. Sundarababu, S. S. Anandan & P. Griskevicius, "Evaluation of mechanical properties of biodegradable coconut shell/rice husk powder polymer composites for light weight applications", Materials Today: Proceedings **39** (2021) 1241. https://doi.org/10.1016/j.matpr.2020.04.095.

[12] M. A. Suhot, M. Z. Hassan, S. A. A. Aziz & M. Y. Md Daud, "Recent progress of rice husk reinforced polymer composites: A review", Polymers **13** (2021) 2391. https://doi.org/10.3390/polym13152391.

[13] R. Premkumar, R. R. Babu, V. S. Jatti & V. SN, "Coconut fiber reinforced with wood charcoal, egg shell filler powder with polyester resin composite for automotive applications", Next Research **2** (2025) 100414. https://doi.org/10.1016/j.nexres.2025.100414.

[14] S. Radhakrishnan, J. S. Krishna, S. P. Dwivedi, S. Gupta, P. Gupta & V. Chaudhary, "Experimental investigation of mechanical and physical properties of coconut shell and eggshell filler-based bio-fiber reinforced epoxy hybrid composites", Biomass Conversion and Biorefinery **15** (2025) 3201. https://doi.org/10.1007/s13399-023-05037-4.

[15] X. Li, L. G. Tabil & S. Panigrahi, "Chemical treatments of natural fiber for use in natural fiber-reinforced composites: a review", Journal of Polymers and the Environment **15** (2007) 25. https://doi.org/10.1007/s10924-006-0042-3.

[16] M. M. Ruma, A. M. A. Badr, S. Khater & A. M. M. El-tantawi, "Assessment of some physicochemical parameters levels in sachet drinking water and its effects on human health in Katsina Urban Area, Nigeria", Science World Journal **9** (2014) 19. https://doi.org/10.4314/swj.v9i1.3.

[17] B. O. Samuel, "Manufacturing parameters optimization and modeling of PxGyEz hybrid composite for high flexural strength using Taguchi robust experimental design technique and general regression analysis", Research Square (2021). Preprint. [Online]. https://doi.org/10.21203/rs.3.rs-831643/v1.

[18] A. Balaji, S. Kannan, R. Purushothaman, S. Mohanakannan, A. H. Maideen, J. Swaminathan, B. Karthikeyan & P. Premkumar, "Banana fiber and particle-reinforced epoxy biocomposites: mechanical, water absorption, and thermal properties investigation", Biomass Conversion and Biorefinery **14** (2024) 7835. https://doi.org/10.1007/s13399-022-02829-y.

[19] R. Kenneth, K. M. Kalu, N. A. Haruna, E. K. Chinedu, I. Atiku & M. Emmanuel, "Baobab (Adansonia digitata) pulp and mango seeds as new adsorbents for the removal of Pb (II) ions from aqueous solutions", Asian Journal of Chemical Science **13** (2023) 13. https://doi.org/10.9734/ajocs/2023/v13i6277.

[20] F. Kapile, *Influence of rice husk derived nano-silica on performance, emissions, and combustion characteristics of diesel engine fueled with baobab biodiesel*, Ph.D. dissertation, Nelson Mandela African Institution of Science and Technology, NM-AIST, Tanzania, 2024. https://dspace.nm-aist.ac.tz/bitstream/handle/20.500.12479/2733/PhD_SESE_%20Kapile_Fredrick_2024.pdf?sequence=1.

[21] H. Mao, F. Wang, X. Zhu, X. Chen, W. Li & W. Zhang, "Design of a BaO–Al2O3–SiO2–B2O3 glass-ceramic for microwave LTCC substrate material based on glass-ceramic+ ceramic composite", Journal of Materials Science: Materials in Electronics **33** (2022) 24834. https://doi.org/10.1007/s10854-022-09194-6.

[22] X. Yan, X. Wang, S. Wang, S. Zhang, X. Zhang, Q. Wang & Q. Wang, "Influence of Al2O3/SiO2 and BaO/Al2O3 ratios on rheological and crystallization behavior of CaO–BaO–Al2O3-based mold slags", ISIJ International **62** (2022) 1116. https://doi.org/10.2355/isijinternational.ISIJINT-2021-565.

[23] C. Silva, F. Bobillier, D. Canales, F. Antonella Sepúlveda, A. Cament, N. Amigo, L. M. Rivas, M. T. Ulloa, P. Reyes & J. A. Ortiz, "Mechanical and antimicrobial polyethylene composites with CaO nanoparticles", Polymers **12** (2020) 2132. https://doi.org/10.3390/polym12092132.

[24] A. Akbari, M. Amini, A. Tarassoli, B. Eftekhari-Sis, N. Ghasemian & E. Jabbari, "Transition metal oxide nanoparticles as efficient catalysts in oxidation reactions", Nano-Structures & Nano-Objects **14** (2018) 19. https://doi.org/10.1016/j.nanoso.2018.01.006.

[25] R. van de Krol, Y. Liang & J. Schoonman, "Solar hydrogen production with nanostructured metal oxides", Journal of Materials Chemistry **18** (2008) 2311. https://doi.org/10.1039/B718969A.

[26] W. Lamai, P. Aunbamrung & A. Wongkaew, "Characteristic and catalytic activity of CuO supported over Fe2O3 catalyst for CO removal", International Conference Burapha University, Thailand, 2014. https://www.researchgate.net/publication/295907081_Characteristic_and_Catalytic_activity_of_CuO_supported_over_Fe2O3_catalyst_for_CO_removal/figures?lo=1.

[27] H. Ma, Q. Zhuo & B. Wang, "Characteristics of CuO-MoO3-P2O5 catalyst and its catalytic wet oxidation (CWO) of dye wastewater under extremely mild conditions", Environmental Science & Technology **41** (2007) 7491. https://doi.org/10.1021/es071057p.

[28] W. Han, Q. Shi & R. Hu, "Advances in electrochemical energy devices constructed with tungsten oxide-based nanomaterials", Nanomaterials **11** (2021) 692. https://doi.org/10.3390/nano11030692.

[29] S. G. Krishnan, A. Arulraj, M. Khalid, M. Reddy & R. Jose, "Energy storage in metal cobaltite electrodes: Opportunities & challenges in magnesium cobalt oxide", Renewable and Sustainable Energy Reviews **141** (2021) 110798. https://doi.org/10.1016/j.rser.2021.110798.

[30] S. Chayoukhi, B. Gassoumi, H. Dhifelaoui, A. Boukhachem & M. Amlouk, "Nanomechanical behavior, adhesion and wear resistance of tin oxide coatings for biomedical applications", Materialwissenschaft und Werkstofftechnik **55** (2024) 427. https://doi.org/10.1002/mawe.202300242.

[31] A. Amjad, H. Awais, M. S. Z. Abidin & A. A. A. Rahman, "Effect of Al2O3 and MgO nanofiller on the mechanical behaviour of alkaline-treated jute fibre–reinforced epoxy bio-nanocomposite", Biomass Conversion and Biorefinery **14** (2024) 9749. https://doi.org/10.1007/s13399-022-03032-9.

[32] G. Ascensão, F. Faleschini, M. Marchi, M. Segata, J. Van De Sande, H. Rahier, E. Bernardo & Y. Pontikes, "High-temperature behavior of CaO-FeOx-Al2O3-SiO2-rich alkali activated materials", Applied Sciences **12** (2022) 2572. https://doi.org/10.3390/app12052572.

[33] K. Kaur, R. Kaur & H. Kaur, "A systematic review of lignocellulosic biomass for remediation of environmental pollutants", Applied Surface Science Advances **19** (2024) 100547. https://doi.org/10.1016/j.apsadv.2023.100547.

[34] M. Santiago Cintrón & D. J. Hinchliffe, "FT-IR examination of the development of secondary cell wall in cotton fibers", Fibers **3** (2015) 30. https://doi.org/10.3390/fib3010030.

[35] R. Md Salim, J. Asik & M. S. Sarjadi, "Chemical functional groups of extractives, cellulose and lignin extracted from native Leucaena leucocephala bark", Wood Science and Technology **55** (2021) 295. https://doi.org/10.1007/s00226-020-01258-2.

[36] S. Sukhikh, A. Prosekov, S. Ivanova, P. Maslennikov, A. Andreeva, E. Budenkova, E. Kashirskikh, A. Tcibulnikova, E. Zemliakova & I. Samusev, "Identification of metabolites with antibacterial activities by analyzing the FTIR spectra of microalgae", Life **12** (2022) 1395. https://doi.org/10.3390/life12091395.

[37] Y. Huang, L. Wang, Y. Chao, D. S. Nawawi, T. Akiyama, T. Yokoyama & Y. Matsumoto, "Analysis of lignin aromatic structure in wood based on the IR spectrum", Journal of Wood Chemistry and Technology **32** (2012) 294. https://doi.org/10.1080/02773813.2012.666316.

[38] P. H. F. Pereira, V. Arantes, B. Pereira, H. L. Ornaghi Jr, D. M. De Oliveira, S. H. Santagneli & M. O. H. Cioffi, "Effect of the chemical treatment sequence on pineapple peel fiber: chemical composition and thermal degradation behavior", Cellulose **29** (2022) 8587. https://doi.org/10.1007/s10570-022-04806-0.

[39] P. Olesik, M. Godzierz, M. Kozioł, J. Jała, U. Szeluga & J. Myalski, "Structure and mechanical properties of high-density polyethylene composites reinforced with glassy carbon", Materials **14** (2021) 4024. https://doi.org/10.3390/ma14144024.

[40] M. I. Uzochukwu, W. U. Eze, P. Garba, M. I. Ugbaja & H. Opara, "Study on the physico-mechanical properties of treated baobab fiber (Adansonia Digitata) nano-filler/epoxy composite", Multiscale and Multidisciplinary Modeling, Experiments and Design **3** (2020) 151. https://doi.org/10.1007/s41939-020-00068-0.

[41] N. Saba, M. Jawaid, O. Y. Alothman & M. Paridah, "A review on dynamic mechanical properties of natural fibre reinforced polymer compos-

ites", Construction and Building Materials **106** (2016) 149. https://doi.org/10.1016/j.conbuildmat.2015.12.104.

[42] O. Shakuntala, G. Raghavendra & A. Samir Kumar, ‘‘Effect of filler loading on mechanical and tribological properties of wood apple shell reinforced epoxy composite", Advances in Materials Science and Engineering **2014** (2014) 538651. https://doi.org/10.1155/2014/538651.

[43] J. George, M. Sreekala & S. Thomas, ‘‘A review on interface modification and characterization of natural fiber reinforced plastic composites", Polymer Engineering & Science **41** (2001) 1471. https://doi.org/10.1002/pen.10846.

[44] M. Jawaid & H. A. Khalil, *Cellulosic/synthetic fibre reinforced polymer hybrid composites: A review*, Carbohydrate Polymers **86** (2011) 1. https://doi.org/10.1016/j.carbpol.2011.04.043.

[45] H. A. Rodríguez, W. M. Kriven & H. Casanova, ‘‘Development of mechanical properties in dental resin composite: Effect of filler size and filler aggregation state", Materials Science and Engineering: C **101** (2019) 274. https://doi.org/10.1016/j.msec.2019.03.090.

[46] F. Elfakhri, R. Alkahtani, C. Li & J. Khaliq, ‘‘Influence of filler characteristics on the performance of dental composites: A comprehensive review", Ceramics International **48** (2022) 27280. https://doi.org/10.1016/j.ceramint.2022.06.314.

[47] W. Brostow & H. E. Hagg Lobland, ‘‘Brittleness of materials: implications for composites and a relation to impact strength", Journal of Materials Science **45** (2010) 242. https://doi.org/10.1007/s10853-009-3926-5.

[48] F. Weber, V. Dötschel, P. Steinmann, S. Pfaller & M. Ries, ‘‘Evaluating the impact of filler size and filler content on the stiffness, strength, and toughness of polymer nanocomposites using coarse-grained molecular dynamics", Engineering Fracture Mechanics **307** (2024) 110270. https://doi.org/10.1016/j.engfracmech.2024.110270.

[49] A. Pearson, M. Duncan, A. Hammami & H. E. Naguib, ‘‘Interfacial adhesion and thermal stability of high-density polyethylene glass fiber composites", Composites Science and Technology **227** (2022) 109570. https://doi.org/10.1016/j.compscitech.2022.109570.

[50] K. P. Kaurase & D. Singh, ‘‘Influence of filler content on the mechanical, thermal, moisture absorption, and biodegradability properties of bio-nanocomposite with cellulosic fibers derived from Delonix Regia fruits", Mechanics of Advanced Composite Structures **11** (2024) 73. https://doi.org/10.22075/macs.2023.30248.1491.

[51] R. Sundarakannan, K. Balamurugan, Y. Jyothi, V. Arumugaprabu, T. Sathish, Z. Mahmoud, E. S. Yousef, D. Basheer & S. Shaik, ‘‘Importance of fiber-/nanofiller-based polymer composites in mechanical and erosion performance: A review", Journal of Nanomaterials **2023** (2023) 3528977. https://doi.org/10.1155/2023/3528977.

[52] J. L. Thomason & J. L. Rudeiros-Fernández, ‘‘A review of the impact performance of natural fiber thermoplastic composites", Frontiers in Materials **5** (2018) 60. https://doi.org/10.3389/fmats.2018.00060.

[53] Y. Sun, Y. Zhao, J. Wu, X. Kai, Z. Zhang, Z. Fang & C. Xia, ‘‘Effects of particulate agglomerated degree on deformation behaviors and mechanical properties of in-situ ZrB2 nanoparticles reinforced AA6016 matrix composites by finite element modeling", Materials Research Express **7** (2020) 036507. https://doi.org/10.1088/2053-1591/ab7b27.

[54] R. L. Oréfice, L. L. Hench & A. B. Brennan, ‘‘Effect of particle morphology on the mechanical and thermo-mechanical behavior of polymer composites", Journal of the Brazilian Society of Mechanical Sciences **23** (2001) 1. https://doi.org/10.1590/S0100-73862001000100001.

[55] S. J. Arul, N. M. Basavaraj & J. SP, ‘‘Influence of bio fillers on the characteristics of Luffa acutangula fiber reinforced polymer composites and parametric optimization using Taguchi technique", Scientific Reports **14** (2024) 30730. https://doi.org/10.1038/s41598-024-80316-2.

[56] E. Muñoz & J. A. García-Manrique, ‘‘Water absorption behaviour and its effect on the mechanical properties of flax fibre reinforced bioepoxy composites", International Journal of Polymer Science **2015** (2015) 390275. https://doi.org/10.1155/2015/390275.

[57] J. Su & J. Zhang, ‘‘Comparison of rheological, mechanical, electrical properties of HDPE filled with BaTiO3 with different polar surface tension", Applied Surface Science **388** (2016) 531. https://doi.org/10.1016/j.apsusc.2015.10.156.

[58] E. Kablov & V. Startsev, ‘‘The influence of internal stresses on the aging of polymer composite materials: A review", Mechanics of Composite Materials **57** (2021) 565. https://doi.org/10.1007/s11029-021-09979-6.